J. Water Environ. Nanotechnol., 9(2): 186-195 Spring 2024

ORIGINAL RESEARCH PAPER

The Effect of Particle Size on Photocatalytic Degradation of Oxytetracycline by ZnO Nanoparticles

Reza Torkamani[1], Bagher Aslibeiki[1]*, Masih Darbandi[2], Hamid Naghshara[1]

[1] *Faculty of Physics, University of Tabriz, Tabriz, Iran*
[2] *Nanomaterials Research Laboratory, Department of Physical Chemistry, Faculty of Chemistry, University of Tabriz, Tabriz, Iran*

Received: 2023-12-10 Accepted: 2024-01-05 Published: 2024-05-12

ABSTRACT
The toxicity of oxytetracycline (OTC) antibiotics remains in the environment and threatens the life of living things. In this research, two series of ZnO nanoparticle catalysts with different particle sizes were prepared. The structural and optical characteristics of the samples were analyzed and the photocatalytic degradation of OTC was investigated under a 100 W visible light irradiation. The samples prepared using zinc nitrate and zinc acetate showed different photocatalytic performance. The catalysts prepared at lower calcination temperatures show higher photocatalytic performance due to the active surface of the particles. The intensity of the peaks in the XRD patterns of samples also increases with increasing calcination temperature, which confirms the increase in the size of the nanoparticles. The decrease in particle size with increasing calcination temperature was confirmed by FESEM images. On the other hand, the band gap energy was reduced by decreasing the calcination temperature, which increases the performance of the photocatalytic activity. The 27 nm ZnO nanoparticles prepared using zinc nitrate showed 100 % degradation efficiency. As a result, we reached the maximum performance of pure ZnO by only controlling the size and morphology, without making nanocomposite or doping different elements.

Keywords: *Zinc oxide, Catalysts, Visible light, Oxytetracycline.*

How to cite this article
Torkamani R., Aslibeiki B., Darbandi M., Naghshara H., The Effect of Particle Size on Photocatalytic Degradation of Oxytetracycline by ZnO Nanoparticles. J. Water Environ. Nanotechnol., 2024; 9(2): 186-195.
DOI: 10.22090/jwent.2024.02.05

INTRODUCTION

In recent years, due to the spread of environmental pollution such as organic compounds, antibiotics, and phenolic compounds, it has always been the focus of many researchers to reduce or degrade them from the environment [2, 7, 20, 31]. Antibiotics are organic pollutants that are used by humans and animals to prevent and treat diseases [2, 19, 35, 44]. The tetracycline antibiotics family includes tetracycline, oxytetracycline (OTC), and chlortetracycline [4]. However, the OTC is not degraded by the environment and can be actively excreted from the body and cause environmental pollution [23, 42]. Therefore, it should be degraded using different methods.

There are various methods such as surface adsorption and electrochemical methods for organic pollutants removal from water [29]. One of these eco-friendly methods is the advanced oxidation process. Today, photocatalytic degradation is one of the methods used due to various advantages. In the degradation process, a pure, doped, or composite semiconductor converts organic materials into non-toxic materials such as water and carbon dioxide using free radicals [2, 5, 28]. The process of converting a pollutant such as OTC to CO_2 and H_2O is called mineralization [47]. It is possible to measure the amount of this

* Corresponding Authors Email: *b.aslibeiki@tabrizu.ac.ir*

conversion in this process using experiments. Various materials such as g-C_3N_4, TiO_2, and ZnO have been used [9, 25, 47]. Among semiconductors, ZnO is an n-type semiconductor with an energy gap of 3.37 eV, which is used in various fields, especially photocatalytic activity [22]. Since, ZnO shows unique properties such as high refractive index [3], ultraviolet absorption [12], antibacterial behavior [33], etc., various nanostructures have been prepared using this material. The ZnO nanostructures such as nanoparticles (NPs) [1], nanorods [11, 26, 39], thin films [10, 38], etc. have been prepared for application in photocatalytic activities. In particular, ZnO NPs have been used as photocatalysts due to their high surface/volume ratio, as an essential parameter in this field of study. However, according to the literature, pure ZnO NPs exhibit low photocatalytic performance. Therefore, different doping or preparation of nanocomposites are used to reach higher degradation efficiencies [6, 16, 41, 42] which need more time and precise methods causing more costs. Accordingly, the preparation of pure ZnO NPs with a desired method that shows the highest photocatalytic efficiency can be of benefit. Thermal decomposition is a low-cost, facile, and simple method, and the prepared NPs are almost monodispersed [45]. In this method, the size and morphology of the NPs can be controlled by heating time, annealing temperature, and type of raw materials.

Until now, the effect of using different precursors and calcination temperatures on the properties of ZnO nanoparticles has not been investigated. In this study, ZnO NPs will be synthesized by the thermal decomposition method, and OTC degradation under visible light irradiation will be studied using NPs with different sizes. In the following, we will investigate the effect of precursor type and calcination temperature on the properties of nanoparticles. Then, it is expected to improve the performance of photocatalytic activity by determining the most optimal conditions.**2.**

EXPERIMENTAL

Materials

Zinc nitrate tetrahydrate ($Zn(NO_3)_2.4H_2O$), zinc acetate dihydrate ($Zn(CH_3CO_2)_2{\cdot}2H_2O$), and citric acid anhydrous ($C_6H_8O_7$) were purchased from Merck Company.

Preparing the ZnO NPs

To prepare the ZnO NPs, zinc acetate dihydrate and citric acid anhydrous were mixed with a molar ratio of 1:1, and then they were ground for half an hour to reach a homogenous mixture. Then, the powder was poured into an alumina crucible and calcined for 3 h in a furnace at 400 (A400), 600 (A600), and 800 °C (A800). To study the effect of raw materials, the above steps were repeated by using zinc nitrate tetrahydrate instead of zinc acetate dihydrate and the powder was calcined at 400 (N400), 600 (N600), and 800 °C (N800).

Characterization Techniques

Structural properties and morphology of the samples were studied using a Siemens D500 X-ray diffraction (XRD) diffractometer with wavelength radiation (λ = 1.5406 Å) and a TESCAN MIRA3 field emission scanning electron microscopy (FE-SEM). Investigation of functional groups and molecular bonds was done using a Fourier transform infrared (FT-IR) spectrometer model: JASCO-680 Plus. Determining the amount of carbon, hydrogen, and nitrogen impurities in the samples was done using a CHNS-O Elemental Analyzer model: AT2344. The ultraviolet-visible (UV-Vis) spectrum of the samples was studied by a Shimadzu UV-2450 spectrophotometer.

Photocatalytic Degradation Experiments

The photocatalytic activity of the samples was studied by photodegradation of OTC solution using a 100 W visible light irradiation. The concentration of OTC aqueous solution was 20 ppm, and for each experiment, the 0.1 g catalyst was dispersed in 100 ml of OTC solution. The solution was kept in the dark under a magnetic stirrer to obtain the adsorption and desorption equilibrium. After 30 min, the solution and catalyst were exposed to visible light for 120 min. Samples were taken from the solution at different time intervals. Then they were separated from the catalyst by a centrifuge at a speed of 3100 rpm for 3 min. In the next step, the absorption spectrum of the samples was performed using an Analytik Jena SPECORD 250 UV-Vis spectrophotometer.

RESULTS AND DISCUSSION

Structural Properties

Fig. 1a and b show the XRD pattern of the samples. The analysis in the range 20–80° indicated six main peaks at 31.72°, 34.40°, 36.22°, 47.44°, 56.52° and 62.83° indexed to the (100), (002), (101), (102), (110) and (103) planes, respectively.

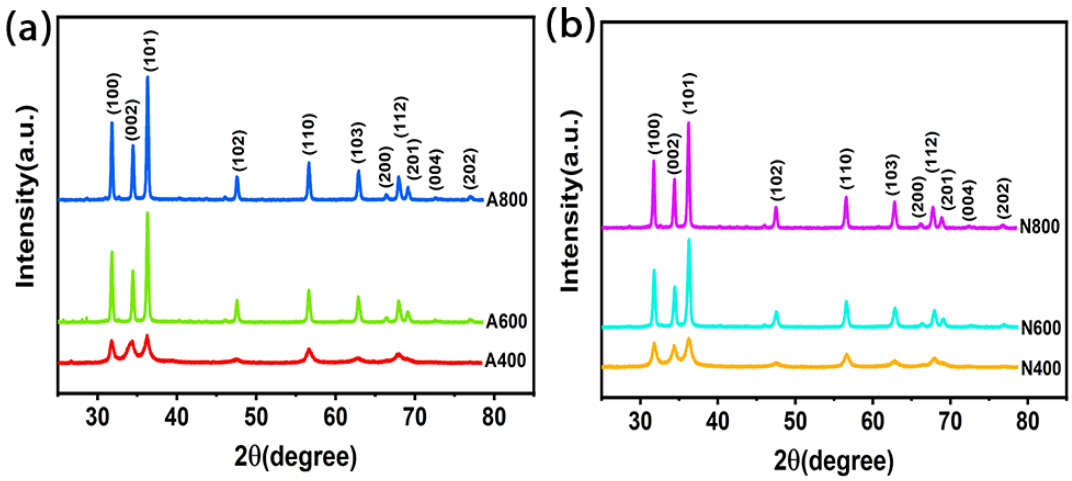

Fig. 1 X-ray diffraction pattern of the ZnO nanoparticles prepared at different calcination temperatures (a) using zinc acetate dehydrate and (b) zinc nitrate tetrahydrate precursors. An increase in the intensity of the peaks in the XRD pattern indicates an increase in the size of the crystallites.

Table 1. Lattice parameters (a,c), unit cell volume (V_{uc}), lattice strain (ε), nanoparticle size obtained from images FESEM ($\langle D\rangle_{SEM}$), and crystal size obtained from Scherer ($\langle D\rangle_{Scherrer}$) and Williamson-Hall ($\langle D\rangle_{W-H}$) equation from the samples.

Parameter	A400	A600	A800	N400	N600	N800
a(Å)	3.25	3.25	3.25	3.25	3.25	3.26
c(Å)	5.24	5.20	5.20	5.22	5.21	5.22
V_{uc}(Å^3)	47.87	47.63	47.59	47.77	47.75	47.91
$\langle D\rangle_{Scherrer}$(nm)	17.40	31.40	36.00	16.42	21.40	27.78
$\langle D\rangle_{W-H}$(nm)	7.30	41.51	41.14	7.41	42.53	53.33
ε	0.00546	0.00058	0.00026	0.00510	0.00178	0.00132
$\langle D\rangle_{SEM}$(nm)	23.10	55.53	75.08	27.33	71.13	171.13

The XRD patterns of the samples were analyzed to check the crystalline phase and impurity using X'Pert software. By comparison with standard diffraction cards, the sample's well-matched card number is 96-230-0113. As shown in Fig. 1a and b, the XRD peaks become sharper as the calcination temperature increases, indicating that the crystalline quality of the samples has increased and the size of the crystallites is bigger. Also, the impurity phase is not seen in the XRD patterns, and all the samples have hexagonal wurtzite structures with a $P6_3mc$ space group.

The lattice parameters (a, c) and volume of the unit cell (V_{uc}) can be obtained using the following equations:

$$\frac{1}{d^2} = \frac{4}{3}\left(\frac{h^2+hk+k^2}{a^2}\right) + \frac{l^2}{c^2} \quad (1)$$

$$V_{uc}=0.866a^2c \quad (2)$$

where h, k, and l are the Miller indices and d is the interplanar distance. In addition, the average crystallite size, $\langle D\rangle_{Scherrer}$, can be calculated using Scherer's equation:

$$\langle D\rangle_{Scherrer} = \frac{K\lambda}{\beta\cos\theta} \quad (3)$$

where K ≅ 0.9 is the Shape factor, λ is the incidence wavelength (1.5406 Å), β is the full width at half-maximum (FWHM) of the XRD peaks, and θ is the Bragg angle. Also, the average crystallite size and lattice strain of the prepared NPs can be calculated using Williamson-Hall's (W-H) formula:

$$\beta\cos\theta = 4\varepsilon\sin\theta + \frac{K\lambda}{\langle D\rangle_{W-H}} \quad (4)$$

where ε is strain, $\langle D\rangle_{W-H}$ is the average crystallite size and β is the total width that includes the width due to the size of the crystals and the width due to ε. As shown in Table 1, the crystallite size

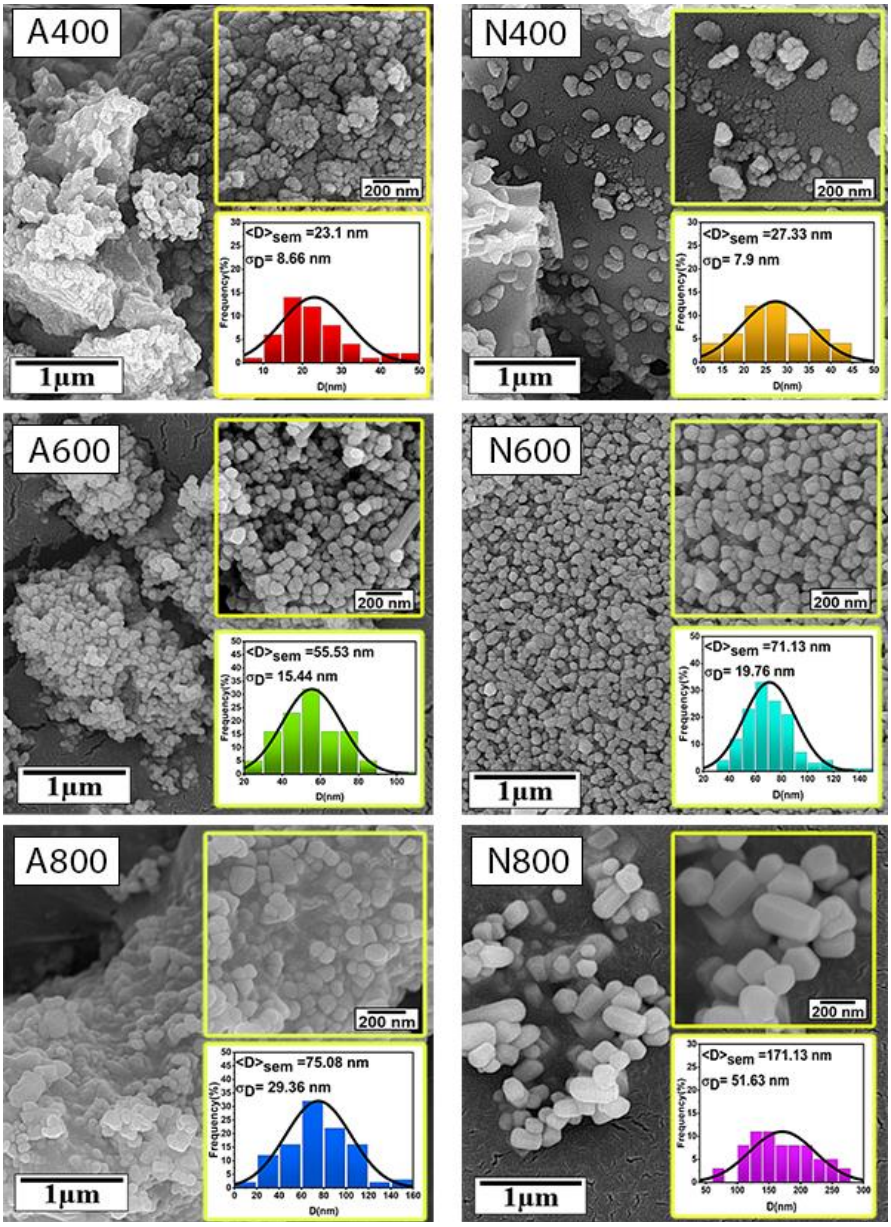

Fig. 2 FE-SEM image and the particle size distribution of ZnO nanoparticles synthesized by thermal decomposition method at different temperatures (400, 600, and 800 °C) with (A400, A600, and A800) zinc acetate dehydrate and (N400, N600, and N800) zinc nitrate tetrahydrate precursors. The particle size distribution indicates an increase in the size of nanoparticles with increasing calcination temperature.

increases with increasing calcination temperature. The prepared NPs with zinc acetate dihydrate have larger crystallite sizes compared to those prepared using nitrate tetrahydrate. At low calcination temperatures, X-ray diffraction peaks of NPs are wider, indicating that the crystalline quality of the samples is lower.

The crystal size obtained for NPs at low calcination temperature using the W-H's formula is smaller than Scherrer's formula. But at high calcination temperatures, this is the opposite. This is related to the change of lattice strain. According to Fig. S1, the W-H's plot has a negative slope at the calcination temperature of 400 °C. But at higher calcination temperatures, the slope of the plot is positive. The negative slope of the plot shows the compressive strain or lattice contraction, and the positive slope of the plot shows the tensile strain

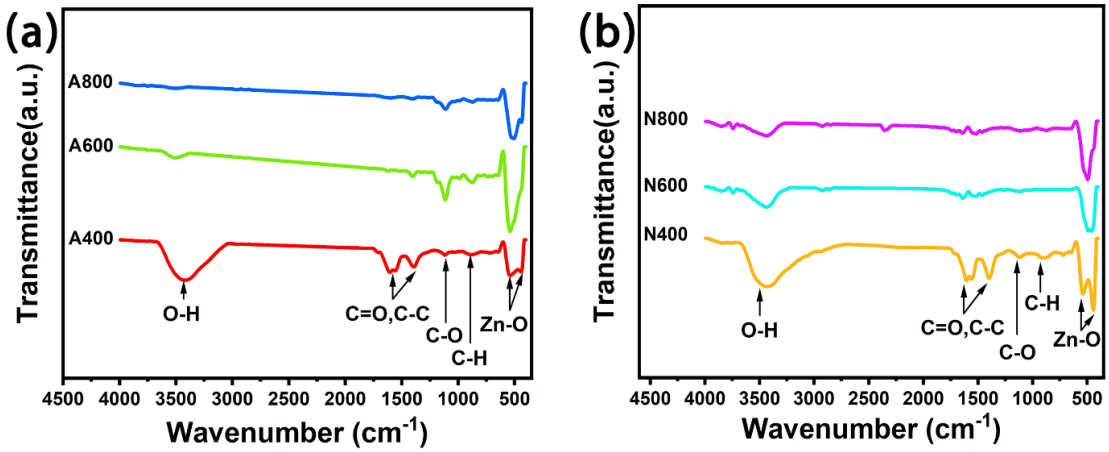

Fig. 3 (a, b) FTIR of as-prepared ZnO nanoparticles at different temperatures and precursors (400, 600, and 800 °C for 3 h with (a)zinc acetate dehydrate (A400, A600, and A800) and (b)zinc nitrate tetrahydrate precursors (N400, N600, and N800)).

[17, 21]. The W-H's formula takes into account the broadening due to lattice strain, but Scherrer's formula does not, therefore the W-H's formula is more accurate than Scherrer's formula. According to Table 1, the obtained lattice constants for NPs are very close to the standard sample (The lattice constants and unit-cell volume of the standard sample are 3.25 Å, 5.21 Å, and 47.72 $Å^3$, respectively).

Morphological Studies

Fig. 2 shows the FE-SEM images of the samples along with the particle size distribution. According to the figure, the NPs are aggregated in some areas. Reducing the particle size increases the surface/volume ratio. Hence, the surface energy increases due to broken bonds on the surface, and NPs aggregate to reduce surface energy. The mean diameter of the particles ($\langle D\rangle_{SEM}$) and the standard deviation (σ_D) were calculated using the following equations:

$$\langle D\rangle_{SEM} = D_0 \exp(\sigma^2/2) \quad (5)$$

$$\sigma_D = \langle D\rangle_{SEM} [\exp(\sigma^2) - 1]^{1/2} \quad (6)$$

According to Table 1, the mean diameter of samples calculated from the FE-SEM image is larger than the $\langle D\rangle_{Scherrer}$ and $\langle D\rangle_{W\text{-}H}$. This indicates that the NPs are composed of several crystallites. According to the average particle size, the samples prepared using zinc acetate dihydrate precursor have a smaller particle size than the NPs prepared with zinc nitrate tetrahydrate precursor. This can be related to the decomposition temperature of the precursor. The decomposition temperature of zinc acetate dihydrate and zinc nitrate tetrahydrate is 237 °C and 125 °C, respectively. The zinc nitrate tetrahydrate decomposes earlier than zinc acetate dihydrate. Therefore, the ZnO phase in the samples prepared using zinc nitrate tetrahydrate precursor grew more than NPs prepared using zinc acetate dihydrate as raw material.

FT-IR Analysis

To investigate the composition, quality, and molecular structure of the samples, FT-IR analysis was performed. The results are illustrated in Fig. 3a and b. According to the figure, the peaks at 441 cm^{-1} and 536 cm^{-1} indicate the Zn-O tetrahedral bond [3, 33]. A broad peak at 3440 cm^{-1} is related to the hydroxyl group O-H, part of which is related to moisture absorbed from the KBr powder used in the experiment, and the other part is related to the hydrophilicity of ZnO [14, 32, 40]. The C-H bond can be found in 908 cm^{-1} and 881 cm^{-1} [34]. Two weak absorption peaks at 1124 and 1462 cm^{-1} indicate C-O and C-C bonds, while the peak located at 1630 cm^{-1} is due to the C=O bond [24, 34].

Also, to determine the amount of carbon, hydrogen, and nitrogen present in the samples, a CHN test was carried out on the A600 sample, indicating the amount of carbon, hydrogen, and nitrogen were 0.31, 0.33, and 0.14%, respectively. These results show that the samples have high purity.

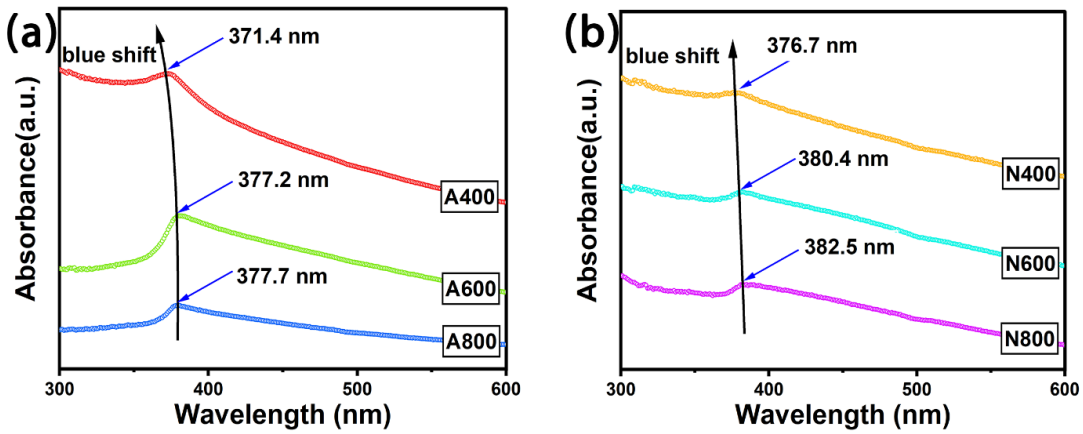

Fig. 4 UV-Vis absorption spectra of as-prepared ZnO nanoparticles with (a) zinc acetate dehydrate (A400, A600, and A800) and (b)zinc nitrate tetrahydrate (N400, N600, and N800) precursors at different calcination temperatures (synthesized with thermal composition in 400, 600, and 800 °C).

Optical Properties

Fig. 4a shows the absorption spectra of the A400, A600, and A800 samples having absorption edges around 371.4, 377.2, and 377.7 nm, respectively. Fig. 4b shows the absorption spectra of the N400, N600, and N800 samples, having absorption edges at around 376.7, 380.4, and 382.5 nm, respectively. The absorption edge position is blue-shifted with decreasing calcination temperature. The band gap energy (E_g) of the samples has been determined by Tauck's formula [13, 36]:

$$(\alpha h\upsilon)^{\frac{1}{n}} = A(\upsilon h - E_g) \quad (7)$$

where A is the band tailing parameter (representing the slope of the Tauc edge), α is the absorption coefficient and hv is the incident photon energy. It is noted that the band gap of ZnO is direct, so the value of n is equal to 0.5.

Fig. S2 shows Tauc's plot of the samples. The values of the band gap of the prepared NPs are included in Table 2, implying that the energy band gap decreases with increasing the calcination temperature. The increase in particle size could be the possible reason for the decrease in the energy band gap. The lower energy band gap of NPs compared to the bulk sample (3.37 eV) can be due to the existence of inherent defects in the samples [45].

Photocatalytic Activity

The photocatalytic performances of the NPs were investigated under visible light irradiation. Fig. 5a and b show the photodegradation rate of OTC by the prepared NPs with zinc acetate dihydrate and zinc nitrate tetrahydrate, respectively. The degradation percentage of the OTC was obtained by using the following equation [2, 27]:

$$\text{Photocatalytic activity}(\%) = \frac{C_0 - C}{C_0} \times 100 \quad (8)$$

where C_0 and C are the pollutant concentrations at the beginning and after the light radiation, respectively. As shown in Fig. 5e and Table 2, degradation of the OTC for A400, A600, and A800 was 98.99%, 75.17%, and 73.72%, respectively, and for N400, N600, and N800, it was 100%, 83.44%, and 62.81%, respectively. According to these results, it can be seen that the photocatalytic performance decreases by increasing the calcination temperature for both series of samples. Many studies have demonstrated that the size of ZnO nanoparticles increases with the increase of calcination temperature [8]. When the calcination temperature increases, the precursors decompose faster. As a result, there will be more time for the ZnO phase to form. In this way, by increasing the growth of crystallites, larger nanoparticles will be formed. By increasing the particle size and then decreasing the surface/volume ratio, the contact area of NPs with their surrounding environment reduces, and the photocatalytic activity will decrease.

The photocatalytic efficiency of the samples was investigated using pseudo-first-order kinetics. For this purpose, the following equation was used [18]:

$$X = Ae^{-Kt} + E \quad (9)$$

where K is the constant rate (min^{-1}), A is the

Table 2 The optical band gap, degradation degree, and the reaction rate coefficient of the powders.

Parameter	A400	A600	A800	N400	N600	N800
Band gap (eV)	3.091	3.015	3.014	2.970	2.940	2.680
Degradation (%)	98.99	75.17	73.72	100	83.45	62.81
K (min^{-1})	0.0872±0.006	0.0441±0.002	0.0396±0.003	0.0337±0.004	0.1389±0.050	0.0783±0.009

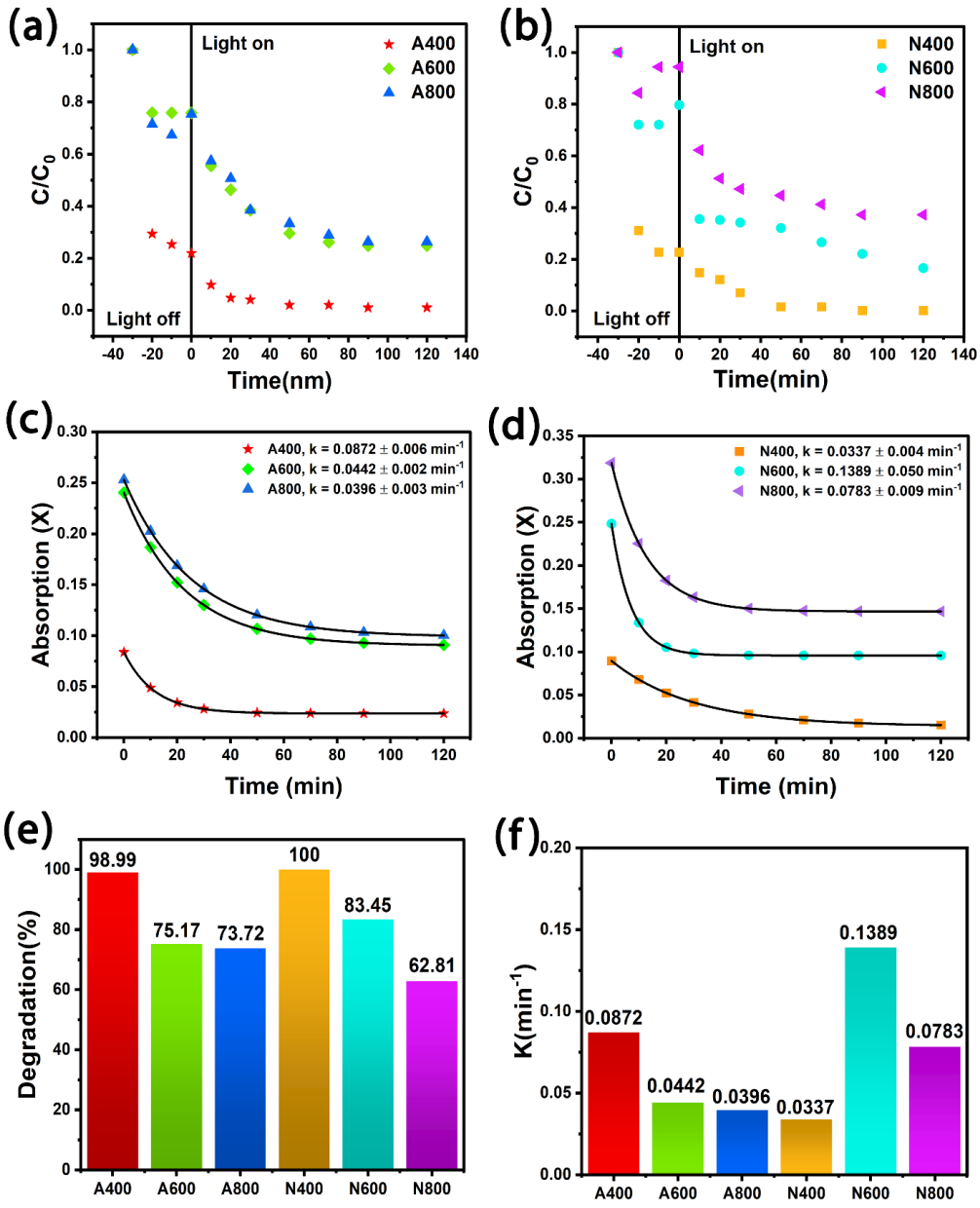

Fig. 5 (a, b) Oxytetracycline degradation under visible light irradiation; (c, d) the non-linear kinetic plots of pseudo-first-order reaction. (e, f) Photodegradation degree and photocatalytic rate of ZnO nanoparticles prepared with zinc acetate dehydrate and zinc nitrate tetrahydrate precursors at different calcination temperatures (400, 600, and 800 °C). The catalyst dose is 1 g/L; oxytetracycline dose 20 ppm; irradiation time 120mins.

amplitude, t is the time of sampling the solution, X is an instrumental signal that is used instead of concentrations and E is the endpoint (is equal to zero in first-order reaction). In Fig. 5c and d, the non-linear fitting of the pseudo-first-order reaction of the samples is shown. Fig. 5f and Table 2, show the kinetic rate obtained from the linear fitting of the samples. According to Fig. 5f, the kinetic rate obtained for N600 is higher than other samples.

According to the literature, the synergistic effect of impurity and zinc, oxygen vacancies, particle size, and the recombination rate are the effective parameters in photocatalytic activities [15, 37, 41].

According to Fig. 5 a and b, it can be seen that the samples prepared with a low calcination temperature before applying light indicate a significant amount of pollutant absorption by the photocatalyst. This is due to the high surface-to-volume ratio as well as the dense structure of the samples. With the separation process, the absorbed amount of pollutant is removed from the solution, and as a result, a small amount of the pollutant remains in the solution for photodegradation. Also, since the amount of K is considered from the time of light application (Fig. 5c and d), the amount of K obtained for the samples prepared with a calcination temperature of 400 °C will be lower. Therefore, N400 and A400 samples show a higher absorption value than other samples.

Oxygen vacancy defects ($V_{\ddot{O}}$) and Zn_i defects in ZnO nanocrystals suppress electron-hole recombination. Defects $V_{\ddot{O}}$ can easily act as electron acceptors to form a single-charge electron ($V_{\dot{O}}$) and simultaneously trap the produced photoholes, thus preventing the recombination of electron-hole [46]. In ZnO nanocrystals, it can be imagined that Zn_i defects act as surface donors. Hence, Zn_i defects can increase photocatalytic performance. The photocatalytic reaction process can be written as follows [43]:

$$ZnO + h\nu \rightarrow e^- + h^+ \quad (10)$$

$$V_{\ddot{O}} + e^- \rightarrow V_{\dot{O}} \quad (11)$$

$$V_{\dot{O}} + O_2 \rightarrow V_{\ddot{O}} + {}^{\cdot}O_2^- \quad (12)$$

$$Zn_i + h^+ \rightarrow Zn_i^+ \quad (13)$$

$$Zn_i^+ + OH^- \rightarrow Zn_i + {}^{\cdot}OH \quad (14)$$

According to the above equations, the produced free radicals (·OH and $^{\cdot}O_2^-$) can cause the degradation of OTC or organic compounds [30]. Therefore, the presence of defects in nanoparticles can affect the photocatalytic performance.

Fig. S3 shows the proposed mechanism for photocatalytic activity. When a light source with energy higher than the energy band gap is irradiated on the powders, the electron-hole pairs (called exciton) are created. The formed excitons can generate free radicals and degrade the pollutants. According to Fig. S3, the crystal defects can act as centers to suppress the electron-hole recombination and increase the degradation efficiency. Thus, a pure ZnO NPs sample with a controlled size can show 100 % degradation efficiency, as was observed for the N400 sample.

As mentioned before, nanoparticles can have more widespread applications in the future due to their high surface-to-volume ratio compared to other ZnO nanostructures. Also, due to its optical properties, non-toxicity, and low cost of its preparation, it can be used in a wide range of applications in the environment in the future. In this research, we were able to increase the photocatalytic efficiency of nanoparticles to 100% by controlling the morphology and energy band gap. This research provides a quick, easy, and cost-effective way to use in the relevant field. Therefore, according to the results of this work, ZnO NPs can be used at the industrial level for purifying polluted water.

CONCLUSION

In summary, the photocatalytic activity, structural, and optical properties of ZnO NPs were investigated. The effect of calcination temperature, particle size, and raw materials were deeply studied through different characterizations. By decreasing the calcination temperature, the intensity of the XRD pattern peaks of the samples decreases. Therefore, it can be concluded that reducing the intensity of the peaks has a direct effect on the morphology of the samples. A blue shift in UV-Vis spectra was observed due to a size reduction, which shows a variation in the band gap. Also, the energy band gap increases with increasing calcination temperature. On the other hand, the photocatalytic performance was low for the samples prepared at high calcination temperatures. As a result, the sample with a lower energy gap shows more appropriate photocatalytic performance. The

sample prepared using zinc nitrate and a calcination temperature of 400 °C showed the maximum photocatalytic efficiency and 100 % degradation of oxytetracycline. The increase in photocatalytic efficiency was related to particle size, surface effects, morphology, and the presence of defects.

REFERENCES

[1] H. Abdullahi Ari, A.O. Adewole, A.Y. Ugya, O.H. Asipita, M.A. Musa, W. Feng, Environmental Technology, 44(9) (2021) 1351. https://doi.org/10.1080/09593330.2021.2001049

[2] M. Ahmadi, H.R. Motlagh, N. Jaafarzadeh, A. Mostoufi, R. Saeedi, G. Barzegar, S. Jorfi, Journal of environmental management, 186 (2017) 55. https://doi.org/10.1016/j.jenvman.2016.09.088

[3] M. Al-Kuhaili, S. Durrani, A. El-Said, R. Heller, Journal of Alloys and Compounds, 690 (2017) 453. https://doi.org/10.1016/j.jallcom.2016.08.165

[4] J.P. Bound, N. Voulvoulis, Water Research, 40 (2006) 2885. https://doi.org/10.1016/j.watres.2006.05.036

[5] T. Chankhanittha, C. Yenjai, S. Nanan, Catalysis Today, 384 (2022) 279. https://doi.org/10.1016/j.cattod.2021.03.002

[6] L.A. Chanu, W.J. Singh, K.J. Singh, K.N. Devi, Results in Physics, 12 (2019) 1230. https://doi.org/10.1016/j.rinp.2018.12.089

[7] D. Cheng, X. Liu, S. Zhao, B. Cui, J. Bai, Z. Li, Science of the Total Environment, 578 (2017) 649. https://doi.org/10.1016/j.scitotenv.2016.11.012

[8] X. Cui, L. Wang, Q. Dong, W. Liang, S. Zhao, Ceramics International, 48 (2022) 34084. https://doi.org/10.1016/j.ceramint.2022.08.165

[9] N. Daneshvar, S. Aber, M.S. Dorraji, A. Khataee, M. Rasoulifard, evaluation, 900 (2007) 6.

[10] A. Di Mauro, M.E. Fragala, V. Privitera, G. Impellizzeri, Materials Science in Semiconductor Processing, 69 (2017) 44. https://doi.org/10.1016/j.mssp.2017.03.029

[11] S. Fathi, B. Aslibeiki, R. Torkamani, Journal of Water and Environmental Nanotechnology, 8 (2023) 254.

[12] E. Goh, X. Xu, P. McCormick, Scripta Materialia, 78 (2014) 49. https://doi.org/10.1016/j.scriptamat.2014.01.033

[13] C. Han, L. Duan, X. Zhao, Z. Hu, Y. Niu, W. Geng, Journal of Alloys and Compounds, 770 (2019) 854. https://doi.org/10.1016/j.jallcom.2018.08.217

[14] S. Hosseini, I.A. Sarsari, P. Kameli, H. Salamati, Journal of Alloys and Compounds, 640 (2015) 408. https://doi.org/10.1016/j.jallcom.2015.03.136

[15] A. Kadam, T.G. Kim, D.S. Shin, K. Garadkar, J. Park, Journal of Alloys and Compounds, 710 (2017) 102. https://doi.org/10.1016/j.jallcom.2017.03.150

[16] M.M. Khan, S. Kumar, A.N. Alhazaa, M. Al-Gawati, Materials Science in Semiconductor Processing, 87 (2018) 134. https://doi.org/10.1016/j.mssp.2018.07.016

[17] D. Kumar, A. Kumar, R. Prakash, A.K. Singh, X-ray diffraction analysis of Cu2+ doped Zn1-xCuxFe2O4 spinel nanoparticles using Williamson-Hall plot method, AIP Conference Proceedings, AIP Publishing LLC, 2019, pp. 070018. https://doi.org/10.1063/1.5122410

[18] G. Lente, Current Opinion in Chemical Engineering, 21 (2018) 76. https://doi.org/10.1016/j.coche.2018.03.007

[19] Z.-j. LI, W.-n. QI, F. Yao, Y.-w. LIU, S. Ebrahim, L. Jian, Journal of Integrative Agriculture, 18 (2019) 1953. https://doi.org/10.1016/S2095-3119(18)62121-5

[20] C. Ma, W.C. Seo, J. Lee, Y. Kim, H. Jung, W. Yang, Chemosphere, 275 (2021) 130052. https://doi.org/10.1016/j.chemosphere.2021.130052

[21] C. Murugesan, G. Chandrasekaran, RSC advances, 5 (2015) 73714. https://doi.org/10.1039/C5RA14351A

[22] C.B. Ong, L.Y. Ng, A.W. Mohammad, Renewable and Sustainable Energy Reviews, 81 (2018) 536. https://doi.org/10.1016/j.rser.2017.08.020

[23] X. Pan, Z. Qiang, W. Ben, M. Chen, Chemosphere, 84 (2011) 695. https://doi.org/10.1016/j.chemosphere.2011.03.022

[24] P. Panchal, D.R. Paul, A. Sharma, P. Choudhary, P. Meena, S. Nehra, Journal of colloid and interface science, 563 (2020) 370. https://doi.org/10.1016/j.jcis.2019.12.079

[25] D.R. Paul, S. Gautam, P. Panchal, S.P. Nehra, P. Choudhary, A. Sharma, ACS omega, 5 (2020) 3828. https://doi.org/10.1021/acsomega.9b02688

[26] N.D. Raskar, D.V. Dake, V.A. Mane, E. Stathatos, U. Deshpande, B. Dole, Journal of Materials Science: Materials in Electronics, 30 (2019) 10886. https://doi.org/10.1007/s10854-019-01433-7

[27] M. Saghi, A. Shokri, A. Arastehnodeh, M. Khazaeinejad, A. Nozari, Journal of Nanoanalysis, 5 (2018) 163

[28] T. Sansenya, N. Masri, T. Chankhanittha, T. Senasu, J. Piriyanon, S. Mukdasai, S. Nanan, Journal of Physics and Chemistry of Solids, 160 (2022) 110353. https://doi.org/10.1016/j.jpcs.2021.110353

[29] A. Shokri, Chemosphere, 296 (2022) 133817. https://doi.org/10.1016/j.chemosphere.2022.133817

[30] A. Shokri, Environmental Challenges, 5 (2021) 100332. https://doi.org/10.1016/j.envc.2021.100332

[31] A. Shokri, International Journal of Environmental Analytical Chemistry, 102 (2022) 5077. https://doi.org/10.1080/03067319.2020.1791328

[32] A. Shokri, Surfaces and Interfaces, 21 (2020) 100705. https://doi.org/10.1016/j.surfin.2020.100705

[33] A. Sirelkhatim, S. Mahmud, A. Seeni, N.H.M. Kaus, L.C. Ann, S.K.M. Bakhori, H. Hasan, D. Mohamad, Nano-micro letters, 7 (2015) 219. https://doi.org/10.1007/s40820-015-0040-x

[34] S.N.A.M. Sukri, K. Shameli, M.M.-T. Wong, S.-Y. Teow, J. Chew, N.A. Ismail, Journal of Molecular Structure, 1189 (2019) 57. https://doi.org/10.1016/j.molstruc.2019.04.026

[35] D. Toloman, A. Popa, M. Stan, M. Stefan, G. Vlad, S. Ulinici, G. Baisan, T.D. Silipas, S. Macavei, C. Leostean, Journal of Alloys and Compounds, 866 (2021) 159010. https://doi.org/10.1016/j.jallcom.2021.159010

[36] R. Torkamani, B. Aslibeiki, Journal of Crystal Growth, DOI (2023) 127317. https://doi.org/10.1016/j.jcrysgro.2023.127317

[37] R. Torkamani, B. Aslibeiki, S. Fathi, Reaction Kinetics, Mechanisms and Catalysis, 136 (2023) 2737. https://doi.org/10.1007/s11144-023-02477-x

[38] R. Torkamani, B. Aslibeiki, H. Naghshara, M. Darbandi, Journal of Interfaces, Thin Films, and Low dimensional systems, 6 (2022) 603.

[39] R. Torkamani, B. Aslibeiki, H. Naghshara, M. Darbandi, Optical Materials, 127 (2022) 112295. https://doi.org/10.1016/j.optmat.2022.112295

[40] P. Uthirakumar, B. Karunagaran, S. Nagarajan, E.-K. Suh,

C.-H. Hong, Journal of crystal growth, 304 (2007) 150. https://doi.org/10.1016/j.jcrysgro.2007.01.035
[41] V. Vaiano, G. Iervolino, L. Rizzo, Applied Catalysis B: Environmental, 238 (2018) 471. https://doi.org/10.1016/j.apcatb.2018.07.026
[42] A.I. Vaizoğullar, Materials Technology, 34 (2019) 433. https://doi.org/10.1080/10667857.2019.1574287
[43] Y. Wang, T. Liu, Q. Huang, C. Wu, D. Shan, Journal of Materials Research, 31 (2016) 2317. https://doi.org/10.1557/jmr.2016.137
[44] K. Wannakan, K. Khansamrit, T. Senasu, T. Chankhanittha, S. Nanan, Antibiotics, 11 (2022) 1590. https://doi.org/10.3390/antibiotics11111590
[45] S. Zandi, P. Kameli, H. Salamati, H. Ahmadvand, M. Hakimi, Physica B: Condensed Matter, 406 (2011) 3215. https://doi.org/10.1016/j.physb.2011.05.026
[46] Y. Zheng, C. Chen, Y. Zhan, X. Lin, Q. Zheng, K. Wei, J. Zhu, Y. Zhu, Inorganic chemistry, 46 (2007) 6675. https://doi.org/10.1021/ic062394m
[47] S. Ziaalmolki, B. Aslibeiki, M. Zarei, R. Torkamani, T. Sarkar, Materials Today Communications, 37 (2023) 107340. https://doi.org/10.1016/j.mtcomm.2023.107340